J|A|C|S
ARTICLES
Published on Web 02/13/2004

Dynamic Docking and Electron-Transfer between Cytochrome b_5 and a Suite of Myoglobin Surface-Charge Mutants. Introduction of a Functional-Docking Algorithm for Protein−Protein Complexes

Zhao-Xun Liang,[†] Igor V. Kurnikov,[†] Judith M. Nocek,[†] A. Grant Mauk,[‡] David N. Beratan,*[,§] and Brian M. Hoffman*[,†]

Contribution from the Department of Chemistry, Northwestern University, 2145 Sheridan Road, Evanston, Illinois 60208, Department of Biochemistry and Molecular Biology, University of British Columbia, Vancouver, British Columbia V6T 1Z3, Canada, and Departments of Chemistry and Biochemistry, Duke University, Box 90346, Durham, North Carolina 27708

Received August 27, 2003

Abstract: Horse myoglobin (Mb) provides a convenient "workbench" for probing the effects of electrostatics on binding and reactivity in the dynamic [Mb, cytochrome b_5] electron-transfer (ET) complex. We have combined mutagenesis and heme neutralization to prepare a suite of six Mb surface-charge variants: the [S92D]Mb and [V67R]Mb mutants introduce additional charges on the "front" face, and incorporation of the heme di-ester into each of these neutralizes the charge on the heme propionates which further increases the positive charge on the "front" face. For this set of mutants, the nominal charge of Mb changes by −1 to +3 units relative to that for native Mb. For each member of this set, we have measured the bimolecular quenching rate constant (k_2) for the photoinitiated ^{3}ZnDMb → $Fe^{3+}b_5$ ET reaction as a function of ionic strength. We find: (i) a dramatic decoupling of binding and reactivity, in which k_2 varies ∼10^3-fold within the suite of Mbs without a significant change in binding affinity; (ii) the ET reaction occurs within the "thermodynamic" or "rapid exchange" limit of the "Dynamic Docking" model, in which a large ensemble of weakly bound protein−protein configurations contribute to binding, but only a few are reactive, as shown by the fact that the zero-ionic-strength bimolecular rate constant varies exponentially with the net charge on Mb; (iii) Brownian dynamic docking profiles allow us to visualize the microscopic basis of dynamic docking. To describe these results we present a new theoretical approach which mathematically combines PATHWAY donor/acceptor coupling calculations with Poisson−Boltzmann-based electrostatics estimates of the docking energetics in a Monte Carlo (MC) sampling framework that is thus specially tailored to the intermolecular ET problem. This procedure is extremely efficient because it targets only the functionally active complex geometries by introducing a "reactivity filter" into the computations themselves, rather than as a subsequent step. This efficiency allows us to employ more computationally expensive and accurate methods to describe the relevant intermolecular interaction energies and the protein-mediated donor/acceptor coupling interactions. It is employed here to compute the changes in the bimolecular rate constant for ET between Mb and cyt b_5 upon variations in the myoglobin surface charge, pH, and ionic strength.

Introduction

Studies of interprotein electron transfer (ET)[1−10] began with the implicit assumption of an energy landscape with a single bound reactive complex, (Figure 1), implying that there is a direct correlation between binding and reactivity. More complex behavior is associated with a landscape having several minima, where the reactive conformation differs from the most stable one. Here, ET kinetics may be controlled by the rates and energetics of conformational conversion within a complex.[11−13] Recent studies of ET between myoglobin (Mb) and cytochrome b_5 (cyt b_5), small globular heme proteins that bind to each other by weak electrostatic interactions disclosed a new paradigm in

[†] Northwestern University.
[‡] University of British Columbia.
[§] Duke University.

(1) Salemme, F. R. *J. Mol. Biol.* **1976**, *102*, 563−568.
(2) McLendon, G.; Hake, R. *Chem. Rev.* **1992**, *92*, 481−490.
(3) Northrup, S. H.; Thomasson, K. A.; Miller, C. M.; Barker, P. D.; Eltis, L. D.; Guillemette, J. G.; Inglis, S. C.; Mauk, A. G. *Biochemistry* **1993**, *32*, 6613−6623.
(4) Nocek, J. M.; Zhou, J. S.; De Forest, S.; Priyadarshy, S.; Beratan, D. N.; Onuchic, J. N.; Hoffman, B. M. *Chem. Rev.* **1996**, *96*, 2459−2489.
(5) Bendall, D. S. *Protein Electron Transfer*; BIOS Scientific Publishers: Oxford, 1996.
(6) Naito, N.; Huang, H.; Sturgess, W.; Nocek, J. M.; Hoffman, B. M. *J. Am. Chem. Soc.* **1998**, *120*, 11256−11262.
(7) Crnogorac, M. M.; Shen, C.; Young, S.; Hansson, Ö.; Kostic, N. M. *Biochemistry* **1996**, *35*, 16465−16474.
(8) Nocek, J. M.; Sishta, B. P.; Cameron, J. C.; Mauk, A. G.; Hoffman, B. M. *J. Am. Chem. Soc.* **1997**, *119*, 2146−2155.
(9) Millett, F.; Durham, B. *Biochemistry* **2002**, *41*, 11315−11324.
(10) Zhu, Z.; Cunane, L. M.; Chen, Z.-W.; Durley, R. C. E.; Mathews, F. S.; Davidson, V. L. *Biochemistry* **1998**, *37*, 17128−17136.
(11) Hoffman, B. M.; Ratner, M. A.; Wallin, S. A. In *Advances in Chemistry Series*; Johnson, M. K., King, R. B., Kurtz, D. M., Jr., Kutal, C., Norton, M. L., Scott, R. A., Eds.; American Chemical Society: Washington, DC, 1990; Vol. 226, pp 125−146.

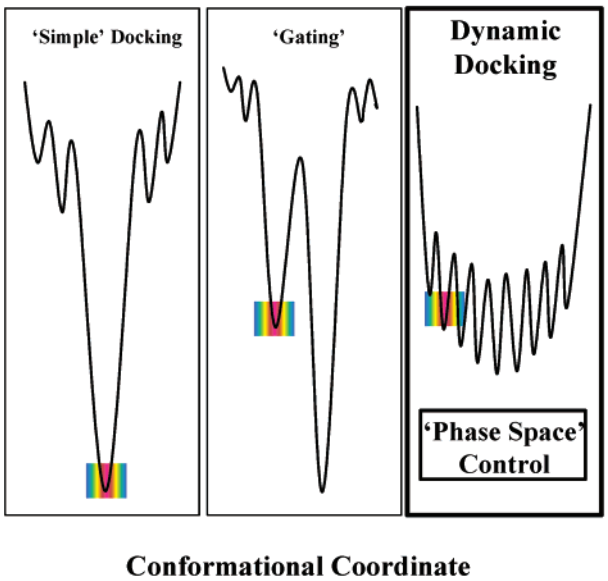

Figure 1. Schematic illustration of the"simple" docking, "gating", and "Dynamic Docking" energy landscapes.

protein−protein reaction dynamics,[14] designated as the "Dynamic Docking" (DD) landscape, in which a large ensemble of weakly bound protein−protein configurations contribute to binding, but only a few are reactive (Figure 1). This introduces a kind of "phase space" control of reactivity in which binding is controlled by the numerous nonreactive configurations, while reaction occurs in the few reactive configurations. A fundamental feature of the DD scheme is that effective ET can occur between partners that are *not* optimized for strong binding. This paradigm was revealed through the observation of a novel decoupling of binding and reactivity: neutralization of the two exposed Mb heme propionates through incorporation of the heme diester[14,15] or, for the first time, the diamide,[16] increased the rate of ET between ZnMb and cyt b_5 by over 2 orders of magnitude without significantly enhancing Mb's binding affinity for cyt b_5.

The ensemble of protein−protein configurations associated with a DD energy landscape each has its own characteristic ET rate constant, k^i_{et}, its own microscopic binding free energy (ΔG_i), and its own binding constant, $K_a{}^i = \exp[-\Delta G_i/kT]$ (which can be expressed in terms of on- and off-rates, k^i_{on}, k^i_{off}, where, $K_a{}^i \propto k^i_{on}/k^i_{off}$). This description likely applies to many weakly bound reacting complexes; as formulated for ZnMb and cyt b_5, the model is described by the kinetic scheme of eq 1.

$$Zn^*Mb + (Fe^{3+})b_5 \left\{ \begin{array}{lll} \overset{K_a{}^1}{\rightleftharpoons} & \{^*ZnMb/b_5\}_1 & \xrightarrow{k_{et}{}^1} \{^+ZnMb/(Fe^{2+})b_5\}_1 \\ \cdots & & \\ \overset{K_a{}^i}{\rightleftharpoons} & \{^*ZnMb/b_5\}_i & \xrightarrow{k_{et}{}^i} \{^+ZnMb/(Fe^{2+})b_5\}_i \\ \cdots & & \\ \overset{K_a{}^j}{\rightleftharpoons} & \{^*ZnMb/b_5\}_j & \xrightarrow{k_{et}{}^j} \{^+ZnMb/(Fe^{2+})b_5\}_j \end{array} \right. \quad (1)$$

The thermodynamic binding constant, K_a, which can be measured in ITC or NMR experiments, or in kinetic titrations at sufficiently high concentrations, is the sum of the individual binding constants ($K_a{}^i$) for all binding conformations (eq 2a).

$$K_a = \sum_i K_a{}^i \quad (2a)$$

With the DD landscape, only a small subset of the many conformations are ET-active; for Mb and cyt b_5, these would be configurations with the hemes of the partners in spatial proximity. However, these do not contribute significantly to binding; if anything, such reactive conformations are disfavored on energetic grounds by electrostatic repulsions between the heme propionates. Thus, the thermodynamic binding constant summation in eq 2a is dominated by the *non*-reactive (NR) majority conformations (eq 2b).

$$K_a \approx \sum_{NR} K_a{}^{NR} \quad (2b)$$

When the concentrations of the two reacting proteins are low compared to the inverse of the binding constant, as in our ET measurements, ET is characterized by a steady-state bimolecular rate constant, k_2. Within the DD model, k_2 can be written as a sum over the simple-docking expressions for each configuration, eq 3a:

$$k_2 = \sum_i k^i_{et} \times k^i_{on}/(k^i_{off} + k^i_{et}) \quad (3a)$$

For the complex between Mb and cyt b_5, we argued[14] that the observed bimolecular ET quenching of the ^{3}ZnMb excited state by $Fe^{3+}b_5$ occurs in the "thermodynamic", or "reaction/fast-exchange limit", where $k^i_{off} \gg k^i_{et}$. In this case, it follows from eq 3a that k_2 is the sum of the ET rate constants for each individual conformation, $k_{et}{}^i$, weighted by the binding constant for that conformation (eq 3b).

$$k_2 = \sum_i k_{et}{}^i K_a{}^i \quad (3b)$$

Because each term in eq 3b is proportional to the rate constant for its configuration, the configurations with small $k_{et}{}^i$ values do not contribute to the overall rate, independent of their contributions to binding. Thus, the summation in eq 3b is, in practice, restricted to reactive (R) conformations (large $k_{et}{}^i$), eq 3c:

$$k_2 \approx \sum_R k_{et}{}^R K_a{}^R \quad (3c)$$

Thus, reactivity and binding are "decoupled": changes in binding probabilities *for the reactive sites* cause equivalent changes in k_2 (eq 3c), yet they can do so without causing corresponding changes in the overall binding constant (eq 2a). Precisely such "decoupling" of binding and reactivity is observed upon neutralization of the two heme propionates of ZnMb,[14] showing that effective bimolecular ET does not require that a protein−protein complex be optimized for strong binding. This may be of physiological relevance for the reduction of met-Mb in muscle and of met-Hb in a red cell, where tight binding

(12) Hoffman, B. M.; Ratner, M. R. *J. Am. Chem. Soc.* **1987**, *109*, 6237−6243.
(13) Pletneva, E. V.; Fulton, D. B.; Kohzuma, T.; Kostic, N. M. *J. Am. Chem. Soc.* **2000**, *122*, 1034−1046.
(14) Liang, Z.-X.; Nocek, J.; Huang, K.; Hayes, R. T.; Kurnikov, I. V.; Beratan, D. N.; Hoffman, B. M. *J. Am. Chem. Soc.* **2002**, *124*, 6849−6859.
(15) Liang, Z.-X.; Nocek, J. M.; Kurnikov, I. V.; Beratan, D. N.; Hoffman, B. M. *J. Am. Chem. Soc.* **2000**, *122*, 3552−3553.
(16) Liang, Z.-X.; Jiang, M.; Ning, Q.; Hoffman, B. M. *JBIC, J. Biol. Inorg. Chem.* **2002**, *7*, 580−588.

Table 1. Bimolecular Rate Constants (k_2) for the Quenching of the Triplets of ZnMb Variants by Cyt b_5 at Low Ionic Strength (pH 7.0, μ = 18 mM, 20 °C)

ZnMb variants	Δq_{nom}[a]	k_2 [M^{-1} s^{-1}]	k_2/k_2(ZnMb)
1 [S92D]ZnMb	−1	7.8×10^5	0.13
2 ZnMb	0	6.1×10^6	1
3 [V67R]ZnMb	+1	8.4×10^7	14
4 [S92D]ZnMb(dme)	+1	4.0×10^7	7
5 ZnMb(dme)	+2	5.5×10^8	90
6 [V67R]ZnMb(dme)	+3	1.4×10^9	230

[a] Nominal change in charge relative to native ferrous or ZnMb.

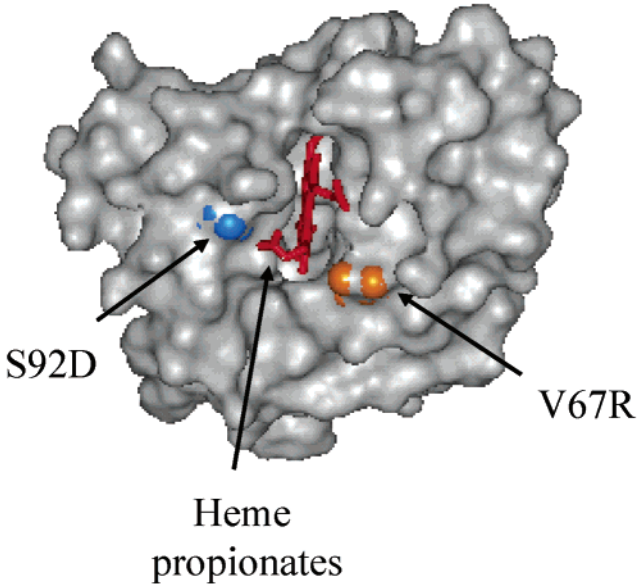

Figure 2. Surface of myoglobin (*horse heart*) designating positions of single-site mutations. Heme is shown with stick rendering to emphasize the solvent exposure of the propionate carboxylates.

of cyt b_5 to the high concentration of ferrous-Mb/Hb would prevent the cytochrome from finding and reducing the oxidized proteins. It likely is of physiological relevance in other situations, as well.

Herein, we broaden the investigation of electrostatic contributions to binding and ET between Mb and cyt b_5, and of the DD model. We employ a suite of Mb surface-charge variants (**1** → **6**, Table 1) prepared by a combination of site-directed mutagenesis and heme neutralization to explore the interplay of docking and electron transfer. We use two Mb mutants: one introduces a negative-charge at position 92 ([S92D]Mb) (nominal charge change, $\Delta q_{nom} = -1$); the other a positive charge at position 67 ([V67R]Mb) ($\Delta q_{nom} = +1$) (Figure 2). By neutralizing the hemes of these two mutants and of the WT Mb as well, we have prepared six Mb variants that nominally differ in charge by an amount ranging from $\Delta q_{nom} = -1$ to +3, as listed in Table 1. These Mbs are turned into photochemical ET donors by substituting Zn for iron in the heme.

This suite of ZnMbs, whose members differ in total charge, local electrostatic potential, and dipole moment, affords an unprecedented tool for studying how interprotein ET is influenced by alterations in the electrostatic interactions between the protein partners. We have determined the bimolecular rate constant (k_2) for the photoinitiated ET reaction and its dependence on salt concentration for each of the six ZnMbs. The results support the key assumptions and predictions of the DD model: multiple weakly bound conformations of the docked complex contribute to the binding of cyt b_5 to Mb, but only a limited subset of these conformations are ET active. They further indicate that reactive binding is electrostatically controlled and that the ET kinetics can be described by the rapid-exchange or "reaction" limit, in which $k^i_{off} \gg k^i_{et}$ and eqs 3b,c hold.

In parallel, we introduce and validate a new "Functional Docking" (FD) approach for calculating interprotein ET rate constants. Typical theoretical treatments of interprotein ET *independently* (i) analyze the reactivity of the partner surfaces through the calculation of surface PATHWAYS coupling maps,[17] and (ii) probe the binding of partners through the use of Brownian Dynamics [3,8,14,16,18,19] or soft docking algorithms[20−23] to generate "docking profiles". Such approaches provide a visualization of the structure and reactivity of docked complexes but do not mathematically integrate the PATHWAYS and docking calculations so as to permit quantitative predictions of bimolecular ET rate constants.

Our new FD procedure for computing ET rate constants mathematically combines the PATHWAY coupling calculations with Poisson−Boltzmann-based electrostatics estimates of the docking energetics in a Monte Carlo (MC) sampling framework that is specially tailored to the intermolecular ET problem. This procedure is more efficient than either the Brownian Dynamics or the soft-docking simulation approaches to describe bimolecular ET in the rapid-equilibration limit because it targets only the functionally active complex geometries by introducing a "reactivity filter" into the computations themselves, rather than as a subsequent step. This efficiency allows us to employ more computationally expensive and accurate methods to describe the relevant intermolecular interaction energies and the protein-mediated donor/acceptor coupling interactions. It is employed here to compute the changes in the bimolecular rate constant for ET between Mb and cyt b_5 upon variations in the myoglobin surface charge and ionic strength.

Materials and Methods

Protein Preparation. Horse heart Mb was purchased from Sigma and further purified by gel-filtration chromatography using a G-75 Sephadex column. Site-directed mutagenesis, expression, and purification of the [S92D]Mb and [V67R]Mb mutants is described elsewhere.[24,25] Zinc deuteroporphyrin IX substituted Mbs (**1**, **2**, **3** in Table 1) and zinc deuteroporphyrin IX dimethylester substituted Mbs (**4**, **5**, and **6** in Table 1) were prepared following the procedures described previously.[8,16] Trypsin-solubilized cyt b_5 was expressed in *Escherichia coli*[26] and further purified by HPLC with an anion-exchange column (Beckman, 21.5 mm × 15 cm, DEAE−5PW) preequilibrated with 20 mM TrisCl, pH 8.0 (20 °C), 0.1 mM EDTA buffer.

ET Kinetic Measurements. Transient absorption kinetics measurements were performed on a laser flash-photolysis apparatus described

(17) Beratan, D. N.; Betts, J. N.; Onuchic, J. N. *Science* **1991**, *252*, 1285−1288.
(18) Eltis, L. D.; Herbert, R. G.; Barker, P. D.; Mauk, A. G.; Northrup, S. H. *Biochemistry* **1991**, *30*, 3663−3674.
(19) Gabdoulline, R. R.; Wade, R. *J. Mol. Biol.* **2001**, *306*, 1139−1155.
(20) Worrall, J. A. R.; Liu, Y.; Crowley, P. B.; Nocek, J.; Hoffman, B. M.; Ubbink, M. *Biochemistry* **2002**, *41*, 11721−11730.
(21) Palma, P. N.; Krippahl, L.; Wampler, J. E.; Moura, J. J. G. *Proteins: Struct., Funct., Genet.* **2000**, *39*, 372−384.
(22) Morelli, X.; Dolla, A.; Czjzek, M.; Palma, P. N.; Blasco, F.; Krippahl, L.; Moura, J. J. G.; Guerlesquin, F. *Biochemistry* **2000**, *39*, 2530−2537.
(23) Morelli, X.; Palma, N.; Guerlesquin, F.; Rigby, A. C. *Protein Sci.* **2001**, *10*, 2131−2137.
(24) Lloyd, E.; Burk, D. L.; Ferrer, J. C.; Maurus, R.; Doran, J.; Carey, P. R.; Brayer, G. D.; Mauk, A. G. *Biochemistry* **1996**, *35*, 11901−11912.
(25) Lloyd, E.; King, b. B. C.; Hawkridge, F. M.; Mauk, A. G. *Inorg. Chem.* **1998**, *37*, 2888−2892.
(26) Funk, W. D.; Lo, T. P.; Mauk, M. R.; Brayer, G. D.; MacGillivray, R. T. A.; Mauk, A. G. *Biochemistry* **1990**, *29*, 5500−5508.

elsewhere.[8] Proteins were exchanged into the desired potassium phosphate buffer using Centricon microconcentrators (Amicon). Anaerobic conditions were achieved by bubbling nitrogen through the buffer solution in a sealed cuvette for ca. 1 h, and gently purging the protein stock solutions with nitrogen for ca. 20 min prior to addition to the cuvette. ET quenching titrations were conducted using ZnMb at a fixed concentration of ~5 μM ($\epsilon_{414\ nm} = 360.8\ mM^{-1}\ cm^{-1}$) and cyt b_5 ($\epsilon_{413\ nm} = 117\ mM^{-1}\ cm^{-1}$)[27] as the quencher at concentrations up to 10 times the concentration of the ZnMb. Ionic strength titrations were carried out by adding aliquots of a concentrated stock solution of NaCl into a buffered solution (10 mM KP, pH 7) containing 5 μM ZnDMb and ~10 μM cyt b_5.

Electrostatic Potential Calculations. The X-ray crystallographic coordinates for horse ferri-Mb (1ymb.pdb)[28] and the trypsin-solubilized fragment of bovine ferri-cyt b_5 (1cyo.pdb)[29] were obtained from the Protein Data Bank. The coordinates for mutants [V67R]Mb (**3**) and [S92D]Mb (**1**) were generated by modifying the coordinates of Mb in DS Viewer Pro software (Accelrys) by "mutating" the appropriate residue; no attempt was made to refine the positions of these surface residues. The coordinates for Mb(dme) (**5**), [V67R]Mb(dme) (**6**), and [S92D]Mb(dme) (**4**) were generated by further adding two methyl groups to the propionates for Mb and the mutants.

Surface electrostatic potentials were calculated by the Poisson−Boltzmann equation as implemented in the program DELPHI that is incorporated in the software GRASP.[30] Default values for the salt concentration (0.0 M), interior dielectric constant (2.0), and exterior dielectric constant (80.0) were used.

Brownian Dynamics (BD) Simulations. Version 3.0.1 of the MacroDox program developed by Northrup and co-workers[3,31] was used to calculate the total charge (q_{net}) and dipole moments (defined according to Koppenol and Margoliash for a protein with arbitrary (nonzero) q_{net} [32]), and to run BD simulations with each of the six mutants. Briefly, charges at pH 7.0 (μ = 18.0 mM) were assigned on the basis of pK_a values derived from a Tanford−Kirkwood calculation.[33,34] Lys and Arg residues were assumed to be fully protonated, while the Asp, Glu, and heme propionates were assumed to be fully dissociated with the charge distributed between the two carboxylate oxygens. The extra positive charges associated with protonation on all the His residues except for the heme ligands were distributed between the N_δ and N_ϵ atoms. The formal charges on the Fe atoms in Mb and cyt b_5 were assigned as +2 and +3, respectively. Poisson−Boltzmann calculations were performed with these charges to determine the electrostatic potential grid surrounding ferrous (or Zn) Mb. In a typical BD run, the simulation starts with the center of cyt b_5 70 Å away from the center of the Mb molecule, with cyt b_5 treated as an array of test charges in the field of Mb without considering cyt b_5's low internal dielectric ("Charges in the Field (CIF)" electrostatic model). The Brownian motion of cyt b_5 in the field of Mb is simulated stochastically by a series of small displacements governed by the Smoluchowski diffusion equation with forces. A trajectory is declared to be reactive or successful if the distance between any of the heme meso-carbons of Mb comes within 25 Å of a heme edge of cyt b_5 at any time before cyt b_5 passes outside an escape radius of 200 Å [35] For each reactive trajectory, the position of cyt b_5 at the instant of contact with the surface of Mb is recorded. A BD simulation generates a docking profile in which the center of mass of cyt b_5 in each hit is displayed as a dot surrounding Mb.

Functional Docking (FD) Calculations. Two models have been used to compute electrostatic energies of protein complexes. One model (the "Charges in the Field" model referred to as the CIF model) computes the protein−protein electrostatic interactions by considering the charges of one protein (cyt b_5) in the electrostatic field of the other (ZnMb); this first field is found through Poisson−Boltzmann calculations of an isolated ZnMb molecule in water. The second model (referred to as the 3PB model) involves Poisson−Boltzmann calculations of the electrostatic energies of the two individual proteins in water and the protein−protein "complex" (configuration) in water for each point of the MC trajectory. The protein−protein electrostatic interaction energy is then computed from the difference of the electrostatic energies of the protein complex and its components.[36]

In 3PB calculations, the protein dielectric constant parameter was set to 4 and the water dielectric constant to 80. A grid of 121 × 121 × 121 was used with zero potential boundary conditions.[37] Atomic charges of the amino acids were assigned from the AMBER force field.[38] PARSE atomic radii and a probe solvent radius of 1.4 Å were used to define a dielectric boundary between protein and water.[39] The interaction between the two proteins were calculated using the CIF model and the excluded volume approximation. In this approximation, the space occupied by atoms of ZnMb is defined by "occupied" points on a rectangular grid. If an atom of the cyt b_5 appears at an "occupied" point, the protein−protein interaction energy is assumed to be very high, and this configuration is excluded from the MC trajectory. Nonbonded interactions between atoms are calculated with the 3PB model. We used the repulsive portion of standard van der Waals potential (B/r^{12}) and the AMBER-94 atomic force-field parameters. The attractive portion of the van der Waals interactions (A/r^6) is discarded to account roughly for nonbonded interactions of the protein with water that is not explicitly present in calculations. The influence of pH on the protein charge was modeled by assigning charges to His residues of Mb and cyt b_5 according to their experimental pK_a values at pH = 7.[40−42]

Results

ET Kinetics. ET from photoexcited ^{3}ZnMbs (**1** → **6**; Table 1) to $Fe^{3+}b_5$ was studied by monitoring the transient absorbance changes of the ^{3}ZnMb at 475 nm. In the absence of cyt b_5, all the ^{3}ZnMb species decay exponentially with the same intrinsic decay rate constant, $k_d = 52 \pm 8\ s^{-1}$. In the presence of cyt b_5, the ^{3}ZnMbs decay remains exponential (rate constant k_{obs})[43] but they are differentially enhanced through quenching by cyt b_5. The quenching rate constants, $k_q = k_{obs} - k_d$, for cyt b_5 quenching of the suite of six ZnMbs at low ionic strength, μ = 18 mM (pH = 7), increase linearly with increasing cyt b_5 concentration, with no indication of saturation (up to [cyt b_5] ≈ 60 μM), Figure 3. The bimolecular quenching rate constant (k_2) is obtained from the slope of a plot of k_q vs [cyt b_5], and the values derived for the data in Figure 3 are presented in Table 1.

The linear variation of k_q (Figure 3**)** is consistent with the low and roughly equal binding constants reported earlier for **2** and **5**,[15,16] which nominally differ in charge through heme

(27) Ozols, J.; Strittmatter, P. *J. Biol. Chem* **1964**, *239*, 1018−1023.
(28) Evans, S. V.; Brayer, G. D. *J. Mol. Biol.* **1990**, *213*, 885−897.
(29) Durley, R. C. E.; Mathews, F. S. *Acta Crystallogr.* **1996**, *D52*, 65−76.
(30) Honig, B.; Nicholls, A. *Science* **1995**, *268*, 1144−1149.
(31) Northrup, S. H.; Boles, J. O.; Reynolds, J. C. L. *Science* **1988**, *241*, 67−70.
(32) Koppenol, W. H.; Margoliash, E. *J. Biol. Chem* **1982**, *257*, 4426−4437.
(33) Matthew, J. B. *Annu. Rev. Biophys. Biophys. Chem.* **1985**, *14*, 387−417.
(34) Tanford, C.; Kirkwood, J. G. *J. Am. Chem. Soc.* **1957**, *79*, 5333−5339.
(35) The use of other criteria for success is illuminating and will be the subject of other reports.
(36) Elcock, A. H.; Sept, D.; McCammon, J. A. *J. Phys. Chem. B* **2001**, *105*, 1504−1518.
(37) Sharp, K. A.; Honig, B. *Annu. Rev. Biophys. Biophys. Chem.* **1990**, *19*, 301−322.
(38) Cornell, W. D.; Cieplak, P.; Bayly, C. I.; Gould, I. R.; Merz, J., K. M.; Ferguson, D. M.; Spellmeyer, D. C.; Fox, T.; Caldwell, J. W.; Kollman, P. A. *J. Am. Chem. Soc.* **1995**, *117*, 5179−5197.
(39) Sitkoff, D.; Sharp, K. A.; Honig, B. *J. Phys. Chem.* **1994**, *98*, 1978−1988.
(40) Bhattacharya, S.; Lecomte, J. T. J. *Biophys. J.* **1997**, *73*, 3241−3256.
(41) McLachlan, S. J.; La Mar, G. N.; Sletten, E. *J. Am. Chem. Soc.* **1986**, *108*, 1285−1291.
(42) Altman, J.; Lipka, J. J.; Kuntz, I. D.; Waskell, L. *Biochemistry* **1989**, *28*, 7516−7523.
(43) More complicated behavior is seen at higher concentrations. This will be described later.

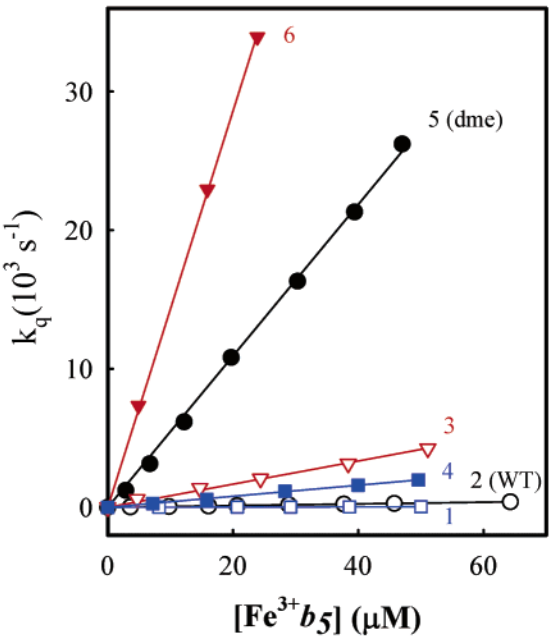

Figure 3. Titration curves for the six Mb variants at 10 mM KP_i (pH 7) μ = 18 mM, 20 °C. *Derivatives*: (□) [S92D]Mb (**1**); (○) Mb (**2**); (▽) [V67R]Mb (**3**); (■) [S92D]Mb(dme) (**4**); (●) Mb(dme) (**5**); (▼) [V67R]-Mb(dme) (**6**).

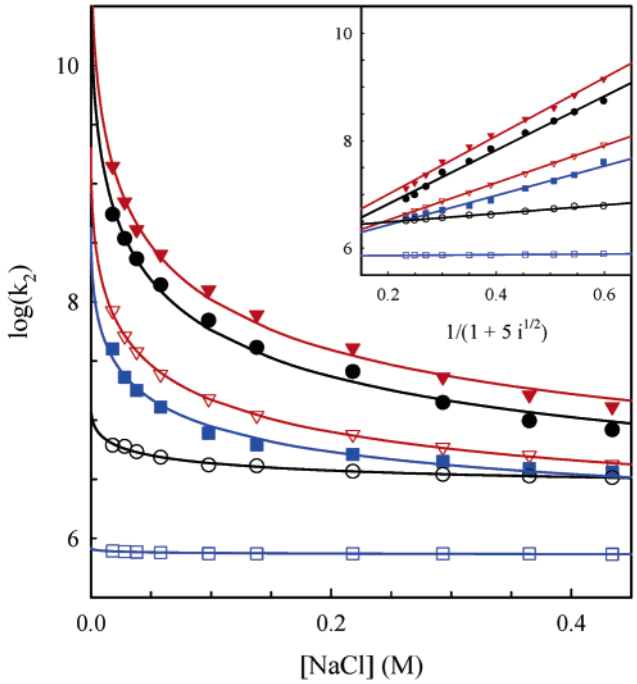

Figure 4. Ionic strength dependence of the log of the bimolecular quenching rate constant, k_2, for Mb's **1**−**6** reacting with cyt b_5. The solid lines are fits to the Debye−Hückel equation (eq 5) as described in the text; the fits assume μ = [NaCl] + 18 mM, as the buffer contribution is μ = 18 mM. *Derivatives*: (□) [S92D]Mb (**1**); (○) Mb (**2**); (▽) [V67R]Mb (**3**); (■) [S92D]-Mb(dme) (**4**); (●) Mb(dme) (**5**); (▼) [V67R]Mb(dme) (**6**). *Conditions*: [Mb] = 5 μM; [cyt b_5] = 10 μM; 10 mM KPi buffer, pH 7.0, 20 °C.

neutralization, by $\Delta q_{nom} = +2$: $K_a(\mathbf{2}) \approx K_a(\mathbf{5}) \lesssim 10^3 M^{-1}$. The linear titration curve for **6** indicates that increasing the charge to $\Delta q_{nom} = +3$ still causes no appreciable increase in K_a. However, the bimolecular rate constant, k_2, increases dramatically from **1** to **6**, Table 1. The value of k_2 decreases 10-fold upon the introduction of a single negative charge on the WT Mb surface at position 92, [S92D]ZnMb (**1**) ($\Delta q_{nom} = -1$). In contrast, introducing a single positive charge ($\Delta q_{nom} = +1$) at position 67, [V67R]ZnMb (**3**), increases k_2 by about 10-fold. A similar, although slightly larger (20-fold), increase is seen for [S92D]ZnMb(dme) (**4**), where the charge change of $\Delta q_{nom} = +1$ is achieved by heme neutralization ($\Delta q_{nom} = +2$) combined with the introduction of a negative charge at position 92. Introduction of a second positive charge, $\Delta q_{nom} = +2$, by methylation of the propionates to yield ZnMb(dme) (**5**) causes a further 10-fold increase in k_2. In contrast, the additional positive charge of [V67R]ZnMb(dme) (**6**) appears to cause a smaller increase, ~3-fold, in k_2. Overall, as the nominal charge varies from $\Delta q_{nom} = -1$ (for [S92D]ZnMb (**1**)) to $\Delta q_{nom} = +3$ (for [V67R]ZnMb(dme) (**6**)), *k_2 increases by more than 3 orders of magnitude*, Table 1.

Figure 4 shows that k_2 is sensitive to salt concentration and that the dependence varies strongly with Δq_{nom}. The quenching constant in all cases decreases with increasing [NaCl], and this decrease is more pronounced as the surface positive charge increases. This behavior is expected for a reaction controlled by electrostatic interactions between ions of opposite charge. While k_2 for WT ZnMb (**2**) shows a significant decrease with [NaCl], the introduction of a negative charge, [S92D]ZnMb (**1**) ($\Delta q_{nom} = -1$) nearly eliminates all such dependence of k_2. Conversely, the introduction of a single positive charge with the [V67R]ZnMb mutant (**3**) ($\Delta q_{nom} = +1$) causes a large increase in sensitivity to ionic strength. Intriguingly, the same net increase in charge ($\Delta q_{nom} = +1$) with [S92D]ZnMb(dme) (**4**) leads to a greater sensitivity than in (**3**), an unsurprising indication that the local-charge distribution, as opposed to the overall charge, does play a significant role.

Electrostatic Calculations. We have calculated electrostatic potential surfaces for the suite of Mbs (Figure S1) and illustrate them in Figure 5 for **1**, **2**, and **6**. Native Mb does not have a distinct "charged patch" near its heme edge where cyt b_5 can dock in ET-active geometries, but rather a "ring" of positive potential around the heme, with a region of negative potential at the heme propionates. The addition of a nearby negative residue, [S92D]ZnMb (**1**), intensifies the negative potential region, whereas increasing the surface positive charge, especially by eliminating the two negative charges of the heme propionates by methylation, progressively enhances the region of positive potential near the heme edge. Obviously, such enhancement of the positive potential near the heme edge of the Mb surface would strengthen the surface electrostatic complementarity for docking cyt b_5 in this surface domain.

In addition, we have calculated the net charge (q_{net}), as well as the direction and magnitude of the total Mb dipole moments as defined by Koppenol and Margoliash[32] for the six Mb variants, Table 2. Tables 1 and 2 show that q_{net} of **1** to **6** varies linearly with the nominal charge, Δq_{nom}; from **1** to **6**, q_{net} varies from −0.9 to 2.2. The span in q_{net} of 3.1, as compared to the span of $\Delta q_{nom} = 4$, indicates that $\Delta q_{net} \propto 0.8\Delta q_{nom}$. This deviation from a slope of one reflects the fact that charge variation influences the pK_a's of acidic and/or basic groups on the surface of the Mbs. Likewise, the Mb dipole moment changes in proportion to Δq_{nom} (Table 2); from **1** to **6**, the magnitude of the total Mb dipole undergoes a 4-fold change from 109 to 431 D; the angle between the Mb dipole vector and the heme α and γ carbon axis changes from 39° to 21°.

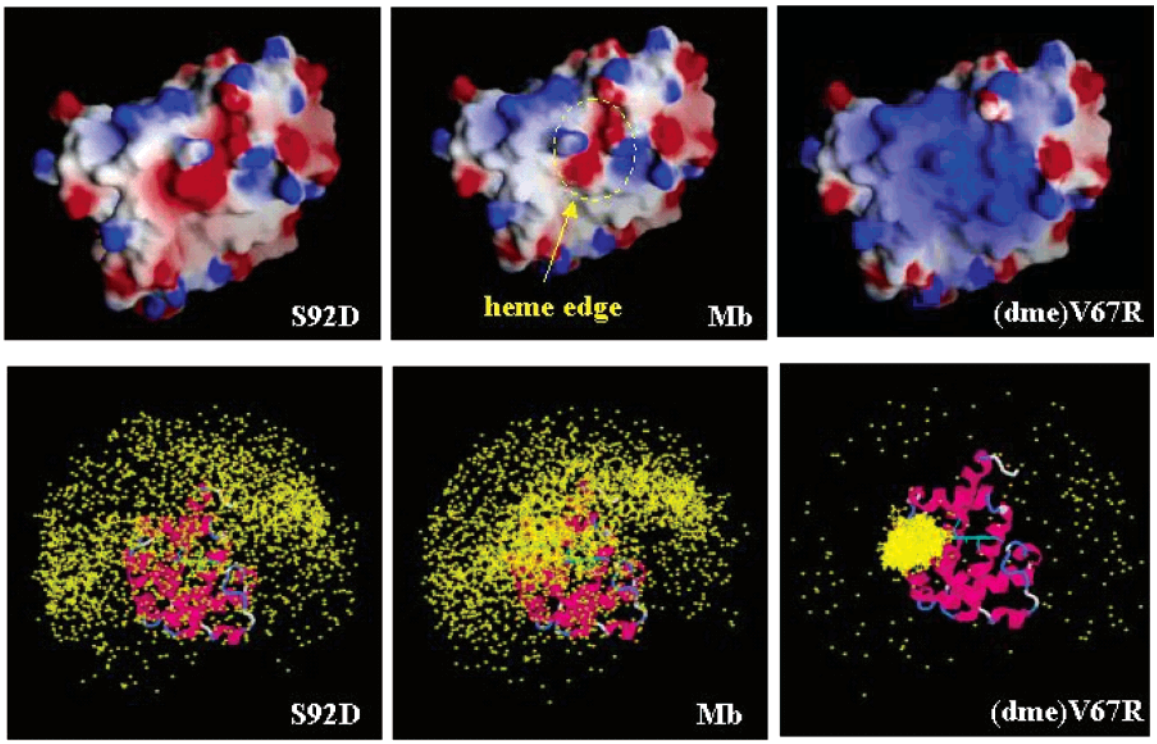

Figure 5. (Top): Electrostatic potential surfaces for Mb (**2**) and its variants, (**1**) and (**6**). The coordinates of Mb variants were generated as described in **Materials and Methods**. The electrostatic potential surfaces were generated with the program GRASP.[30] Color coding: Blue: positive potential; Red: negative potential. (Bottom): Corresponding docking profiles from Brownian Dynamics (BD) simulations. Mbs are represented by ribbons with the heme propionates (cyan) pointing toward the viewer. The *cyt* b_5 centers of mass at points in space where ET criteria are successfully met (heme−heme edge distance less than or equal to 25 Å) are shown with (yellow) dots. The number of complexes generated are: 2055 for **1**, 2573 for **2**, and 3957 for **6**. *Conditions*: pH = 7.0; μ = 18 mM; T = 20 °C.

Table 2. Global Properties of Proteins

protein	Δq_{nm}	q_{net}[a] (e)	dipole[a] (debye)	θ[b] (deg)	effective dipole[c] (debye)
1 [S92D]ZnMb	−1	−0.9	253	38.6	198
2 ZnMb	0	−0.3	293	37.4	233
3 [V67R]ZnMb	+1	0.4	315	32.4	266
4 [S92D]ZnMb(dme)	+1	0.5	331	27.2	294
5 ZnMb(dme)	+2	1.3	385	26.9	343
6 [V67R]ZnMb(dme)	+3	2.2	420	23.3	387
cytochrome b_5		−6.9	500	143	−399

[a] Calculated for pH = 7.0 and μ = 18 mM with MacroDox.[3,31] [b] θ = angle of dipole moment relative to the carbon $\alpha-\gamma$ axis of the Mb heme. [c] Effective dipole (dipole moment along the heme $\alpha-\gamma$ axis) = dipole moment × cos θ.

Brownian Dynamics (BD) Simulations. The docking profiles obtained from BD simulations for the Mb suite are shown in Figure S2; representative examples for **1**, **2**, and **6** are shown in Figure 5. The distribution of cyt b_5 "hits" varies strongly as a function of the nominal charge for the six ZnMbs. Whereas the "hits" form a broad and uniform distribution over the [S92D]-ZnMb surface (**1**), this distribution progressively narrows to a highly localized one for [V67R]Mb(dme) (**6**). In contrast, the total number of cyt b_5 hits (25 Å distance criterion) increases only modestly from 2055 for **1** to 3957 for **6** (for 10^4 total trajectories). In short, the simulations suggest that the binding constant would not change substantially across the suite of Mbs, consistent with observation, while docking near the Mb heme edge becomes progressively more probable. As an alternate way of representing this phenomenon, the average Fe−Fe distance in the docked complexes decreases from 25 to 16 Å going from **1** to **6**.

From among the 2573 "native" [ZnMb (**2**), cyt b_5] complexes generated recently, we found that the structures of the most stable complex (the complex with the most favorable electrostatic energy) and of the putatively most-reactive complex (the complex with the shortest Fe−Zn distance) differ strikingly in donor−acceptor distance and cyt b_5 orientation: the most stable conformation(s) indeed are *not* the most reactive conformation(s).[14] In contrast, we here find that there is only a slight difference between the most stable complex and the most reactive ET complex formed between cyt b_5 and [V67R]ZnMb(dme) (**6**) (data not shown). In short, the results suggest that the surface-charge modifications employed dramatically increase the probability that cyt b_5 binds to the Mb surface in a reactive conformation, near the heme edge.

Theoretical Analysis of ET

We analyze these kinetic results *first* (A) with the Debye−Hückel model for interactions between "simple" ions, and *then* (B) introduce the "Functional Docking" model that integrates a PATHWAY description of protein-mediated coupling with Poisson−Boltzmann computations of protein interaction energies. We use a new Monte Carlo docking procedure that permits us to make quantitative predictions of the intermolecular ET rate changes as a function of the protein structure and solvent properties.

(A) Debye−Hückel Description. Quenching as an Electrostatically Controlled Reaction Between "Simple Ions". Key features of the ET reaction mechanism for cyt b_5 and Mb are revealed by analyzing the ionic strength dependence of the ET kinetics in the context of the Debye−Hückel model.[44,45] In this model, the proteins are represented as charged spheres

Table 3. Parameters from Debye Hückel Fits for the Ionic Strength Dependence of the Bimolecular ET Rate Constant[a]

ZnMb	Δq_{nm}	log k_{20} ($M^{-1}s^{-1}$)	a (C^2)
(**1**) [S92D]Mb	−1	5.9	0.3
(**2**) Mb	0	7.1	3.9
(**3**) [V67R]Mb	+1	9.3	17.4
(**4**) [S92D]Mb(dme)	+1	8.6	13.7
(**5**) Mb(dme)	+2	10.8	25.0
(**6**) [V67R] Mb(dme)	+3	11.3	27.1

[a] pH 7, 20 °C.

interacting in a solution with ionic strength μ and ion diffusion constants, D. In this approximation, the interaction potential between the two ions is[46]

$$V(Z_{Mb}) = \frac{-Z_{Mb}|Z_{cytb5}|\, e^{-\lambda r}}{\epsilon r}$$

$$\lambda^2 = \frac{8\pi^2 e^2 N_o d}{1000\epsilon k_B T}\mu \qquad (4)$$

We emphasize the dependence of V on the Mb charge, Z_{Mb}, and have taken $Z_{b5} < 0$. A limiting equation for the second-order rate constant, k_2, has two contributions and depends on the parameters a and b,[44,45]

$$\ln k_2(Z_{Mb}) = \ln k_{20}(Z_{Mb}) - \frac{a\sqrt{\mu}}{1+b\mu}$$

$$a(Z_{Mb}) = 2.34 Z_{Mb}|Z_{b5}| \qquad (5)$$

$$b = 0.329 R_{av}$$

where $k_{20}(Z_{Mb})$, is the second-order rate constant at zero ionic strength ($\mu = 0$), and we emphasize the explicit dependence of k_{20} on Z_{Mb}. The μ-dependent term reflects the screening of electrostatic interactions by the ionic atmosphere; R_{av} is the average radius of the reactants.

Consider first the dependence of k_2 on added NaCl for the suite of Mb's, Figure 4. To describe the data most simply, we used a 2-parameter fit to eq 5 in which we varied k_{20} and a, while fixing $b = 5$ C; this b value, which was suggested by an initial round of three-parameter fits, corresponds to a reasonable average protein radius, $R_{av} = 15.1$ Å. The resulting two-parameter fits are plotted in Figure 4; the parameters k_{20} and a appear in Table 3. The model's excellent description of the variation of k_2 with [NaCl] confirms that the protein−protein interactions involved in ET-competent binding are primarily controlled by electrostatics.[47−49]

According to the Debye Hückel formula (eq 5), the parameter a should be proportional to the Mb charge. As shown in Table 3, a does indeed increase linearly with Δq_{nom} for the suite of Mbs, and the electrostatic calculations (Table 2) show that the Mb charge varies linearly with Δq_{nom}:$Z_{Mb} \propto q_{net} \propto \Delta q_{nom}$. The ability of the simplified Debye−Hückel equation to describe the ionic-strength dependence satisfactorily for all six ZnMbs confirms that the interaction between Mb and cyt b_5 is indeed dominated by electrostatic attractions.

A minor correction is suggested by the fact that the ionic-strength dependence of k_2 is appreciable for WT Mb (**2**) which is calculated to have $q_{net} \approx 0$ (Table 2), and should thus give $a \rightarrow 0$ and a negligible dependence of k_2 on μ. Instead the dependence is minimal for **1**, which is calculated to have $q_{net} \approx -1$ (Table 2). Computations of q_{net} with experimentally derived pK_a values also give a slightly negative value of q_{net} for WT Mb (∼−0.5e) and a value of −1.5e for the S92D mutant. Thus, an apparent discrepancy between the observed ionic strength dependence for the bimolecular ET rate and the computed total charge of the Mb is not just an error of the Tanford−Kirkwood approach to compute pK_a values for protonation equilibrium. We show below that more accurate calculations with realistic charge distributions and Poisson−Boltzmann electrostatic analysis demonstrate almost flat dependence of the bimolecular ET rate for S92D mutant on ionic strength, although the total charge of this Mb derivative is negative. This apparent contradiction reflects the fact that the nonuniformity of the protein charge distribution plays a major role in Mb/cyt-b_5 electrostatic interactions.

Is the ET Reaction Diffusion Controlled or "Reaction Controlled"? The absence of curvature in the plots of k_2 vs [cyt b_5] (Figure 3**)** is consistent with the occurrence of ET within a weakly bound complex which is in the "reaction limit", $k_{off}{}^i \gg k_{et}{}^i$ (eq 3a), with the reacting partners at low concentrations, as in the present experiments. However, it is also compatible with a diffusion-controlled, bimolecular reaction, corresponding to $k_{off}{}^i \ll k_{et}{}^i$ in eq 3a.[50,51] We now show that the dependence on Mb charge of k_{20} (or the low ionic-strength rate constant as measured for $I = 18$ mM) clearly discriminates between these cases, and supports our previous conclusion [14] that the [Mb, cyt b_5] complex is in the reaction limit.

How does k_{20} depend on Z_{Mb} in the two limits? The rate constant for a diffusion-controlled ET reaction between cyt b_5 and Mb, treated as two charged ions, has the form,[46]

$$k_{20}{}^{dif} \approx 4\pi(D_{Mb} + D_{b5})Z_{Mb}|Z_{b5}| \qquad (6a)$$

where D_{Mb} and D_{b5} are the diffusion coefficients. Thus $k_{20}{}^{dif}$ varies linearly with the charge on ZnMb

$$k_{20}{}^{dif} \approx Z_{Mb} \approx \Delta q_{nom} \qquad (6b)$$

In contrast, the fast-exchange-limit rate constant $k_{20}{}^{fe}$ is proportional to the binding constant for the ET-competent site(s), and thus has the form,[46]

$$k_{20}{}^{fe} \approx k_{et}K_a \propto k_{et}\, e^{-\Delta G^a(Z_{Mb})/kT}$$

$$\approx k_{et}\, e^{-V(Z_{Mb})/kT} \qquad (7a)$$

where ΔG^a, the binding free energy is taken to be the electrostatic binding energy and the second line utilizes the

(44) Sokerina, E. V.; Ullmann, G. M.; Van Pouderoyen, G.; Canters, G. W.; Kostic, N. M. *JBIC, J. Biol. Inorg. Chem.* **1999**, *4*, 111−121.
(45) Zhou, J. S.; Kostic, N. M. *Biochemistry* **1993**, *32*, 4539−4546.
(46) Steinfeld, J. I.; Francisco, J. S.; Hase, W. L. *Chemical Kinetics and Dynamics*; Prentice-Hall: Englewood Cliffs, New Jersey, 1989.
(47) Van Leeuven presented a more sophisticated equation which includes not only the charge−charge interactions but also terms involving charge−dipole and dipole−dipole interactions. Given the success with the simpler function, our conclusions would not change if we used the more complicated function, whose parameters are highly correlated.
(48) Van Leeuwen, J. W. *Biochim. Biophys. Acta* **1983**, *743*, 408−421.
(49) Van Leeuwen, J. W.; Mofers, F. J. M.; Veerman, E. C. I. *Biochim. Biophys. Acta* **1981**, *635*, 434−439.
(50) Schreiber, G. *Curr. Opin. Struct. Biol.* **2002**, *12*, 41−47.
(51) Davidson, V. L. *Acc. Chem. Res.* **2000**, *33*, 87−93.

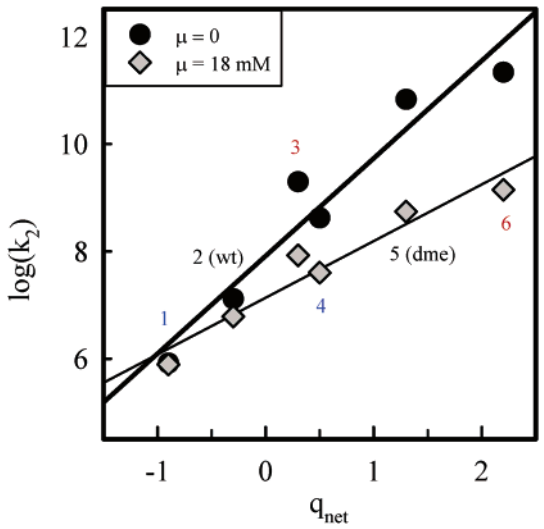

Figure 6. Dependence of the bimolecular rate constant (k_2) on the net charge (q_{net}) for the suite of Mb mutants. (●), $\mu = 0$; (◇), $\mu = 18$ mM.

Debye−Hückel formula, eq 4 for V. Thus, ln k_{20}^{fe} and *not* k_{20}^{fe} would be proportional to Z_{Mb}:

$$\ln k_{20}^{\ fe} \propto Z_{Mb} \propto \Delta q_{nom} \tag{7b}$$

The values of log k_{20} obtained through the fits of eq 5 to the data of Figure 4 are plotted as a function of q_{net} in Figure 6. This figure shows that it is log k_{20}, not k_{20} itself, that increases linearly with q_{net} and thus Z_{Mb}. Equivalently, a plot of log k_2 measured at low ionic strength, $\mu = 18$ mM, varies linearly with q_{net}, and thus Z_{Mb}. The experiments thus clearly show the exponential dependence of k_{20} on the Mb charge predicted to occur when the binding free energy for the reactive conformation(s) is electrostatic in character, eq 7.

(B) Monte Carlo Functional Docking Simulation. Methodology. The *descriptive* Debye−Hückel analysis confirms (i) that the ET kinetics are dominated by electrostatic interactions between Mb and cyt b_5, and (ii) that ET between Mb and cyt b_5 occurs in the thermodynamic, or rapid-exchange limit (eq 7). We now introduce a new "Functional Docking" procedure to compute how the rate of ET between Mb and cyt b_5 changes with variations in the myoglobin surface charge, pH, and/or ionic strength. This approach combines the PATHWAY coupling calculations with Poisson−Boltzmann based electrostatics estimates of the docking energetics in a Monte Carlo sampling framework specially tailored to the intermolecular ET problem.

Imagine an ensemble of boxes of volume V; each box is filled with water, one molecule of ZnMb, and one molecule of cyt b_5. Assume that at some moment all Zn−myoglobin molecules are photo-excited, initiating ET from ^{3}ZnMb to cyt b_5. Further assuming the activation-controlled regime, with rapid pre-equilibrium among all configurations, the ^{3}ZnMb population will decay with unimolecular kinetics,

$$-\mathrm{d}[(\mathrm{ZnP})^3\mathrm{Mb}]/dt = k_{ET}^{Av}[(\mathrm{ZnP})^3\mathrm{Mb}] \tag{8}$$

where k_{ET}^{Av} is the configuration-averaged unimolecular ET rate (eq 9).

$$k_{ET}^{Av} = \sum_i p_i k_{ET}^{\ i} = \sum_i \left[\frac{\exp\left(-\frac{E_i}{k_B T}\right)}{\sum_j \exp\left(-\frac{E_j}{k_B T}\right)} \right] k_{ET}^{\ i} \tag{9}$$

Here $k_{ET}^{\ i}$ is the ET rate constant associated with the ith configuration of the protein pair and E_i is the energy of this configuration. As V becomes small, k_{ET}^{Av} approaches the value of the intracomplex ET rate constant averaged over all conformations of the bound complex, k_{ET}^{DD}

$$k_{ET}^{Av} \xrightarrow{V \text{ small}} k_{ET}^{DD} \tag{10a}$$

In the high dilution (large V) regime, where most configurations are unbound and do not undergo ET, k_{ET}^{DD} becomes the pseudo-first-order ET rate constant, which is related to the second-order bimolecular ET rate constant, k_2 through,

$$k_{ET}^{Av} \xrightarrow{V \text{ large}} k_2[\mathrm{cyt}b_5] \tag{10b}$$

As a result, for high dilution

$$k_2 = k_{ET}^{Av} V \tag{10c}$$

because in our ensemble [cyt b_5]/1/V (concentration in units of particles per unit volume). If one assumes that ET occurs only in bound configurations, k_2 can be written in terms of the binding constants and ET rate constants of the bound configurations (K_a^i; k_{ET}^i) (eq 11), or in terms of the average intracomplex rate constant and the thermodynamic binding constant (k_{ET}^{DD}; K_a) (eq 11):

$$k_2 = \sum_i k_{ET}^{\ i} K_a^{\ i} = k_{ET}^{DD} K_a \tag{11}$$

The expression of eq 11 was used in our previous analysis of the [Mb, cyt b_5] pair.[14] Equations 9−10 are more general, in the sense that they do not introduce explicit partitioning of the configurations into bound and free ones, and the formulation allows nonzero ET rates in ALL protein configurations, regardless of whether they are bound or not.

To focus on only those configurations that contribute to ET, and thus to describe "Functional Docking", we rewrite eq 9 by defining an effective energy that links the interaction energy and the ET rate in the ith configuration (where k^{ref} is a reference ET rate constant which will cancel in the rate ratios considered below):

$$E_i^{\ eff} = E_i - k_B T \ ln(k_{ET}^{\ i}/k^{ref}) \tag{12}$$

With this definition, the configuration-averaged unimolecular ET rate constant for the bimolecular reaction is:

$$k_{ET}^{Av} = \frac{\sum_i \exp\left(-\frac{E_i^{\ eff}}{k_B T}\right)}{\sum_j \exp\left(-\left(\frac{E_j}{k_B T}\right)\right)} \tag{13}$$

The ratio of two ET rates (denoted 1 and 2) measured under different conditions (ionic strength, pH) or for modified proteins (altered hemes, mutated proteins) is:

$$\frac{k_{ET}^{Av}(1)}{k_{ET}^{Av}(2)} = \left(\frac{\sum_i \exp\left(-\frac{E_i^{eff(1)}}{k_B T}\right)}{\sum_i \exp\left(-\frac{E_i^{eff(2)}}{k_B T}\right)}\right)\left(\frac{\sum_j \exp\left(-\frac{E_j^{(2)}}{k_B T}\right)}{\sum_j \exp\left(-\frac{E_j^{(1)}}{k_B T}\right)}\right) \quad (14a)$$

We take the energy zero for ET systems 1 or 2 to be equal to the sum of the energies of the isolated solvated proteins. The second bracket in eq 14a is close to unity in the pseudo-first-order limit (large V of eqs 10b, 10c), where most protein configurations are unbound; this limit holds for the ET reaction between cyt b_5 and Mb in the present experiments. In this limit, eq 14a becomes,

$$\frac{k_{ET}^{Av}(2)}{k_{ET}^{Av}(1)} \rightarrow \frac{k_2(2)}{k_2(1)} = \left[\frac{\sum_i \exp\left(-\frac{E_i^{eff(2)}}{k_B T}\right)}{\sum_i \exp\left(-\frac{E_i^{eff(1)}}{k_B T}\right)}\right] \quad (14b)$$

Equation 14b has the form of a ratio of partition functions for two states with effective state energies $E^{eff(1)}$ and $E^{eff(2)}$. One can introduce an effective free energy $A^{eff}(S)$ for a given state (S) of the system:

$$A^{eff}(S) = -k_B T \ln\left(\sum_i \exp\left(-\frac{E_i^{eff(S)}}{k_B T}\right)\right) \quad (15)$$

The effective free energy definition (eq 15) exactly matches the usual definition of the Helmholtz free energy, **A**, albeit with effective energies $E_i^{eff(S)}$. The ratio of ET rates averaged over configurations (eq 14b) can now be related to the difference in effective free energies:

$$\frac{k_{ET}^{Av}(2)}{k_{ET}^{Av}(1)} \approx \left(\frac{\sum_i \exp\left(-\frac{E_i^{eff(2)}}{k_B T}\right)}{\sum_i \exp\left(-\frac{E_i^{eff(1)}}{k_B T}\right)}\right) \equiv \exp\left(-\frac{A^{eff}(2) - A^{eff}(1)}{k_B T}\right) = \exp\left(-\frac{\Delta A^{eff}(1 \rightarrow 2)}{k_B T}\right) \quad (16)$$

Thus, one can apply free energy perturbation methods and thermodynamic integration to the present problem.[52−55] In this approach, a continuous transition is defined between the configuration energies of the system in the two states (1 and 2), governed by a parameter λ ($0 \le \lambda \le 1$), such that $E_i(\lambda = 0) = E_i(1)$ and $E_i(\lambda = 1) = E_i(2)$. Changes of free energy can be computed using thermodynamic integration.[53,54]

$$\Delta A(1 \rightarrow 2) = \int_{\lambda=0}^{\lambda=1} \left\langle \frac{\partial E_i(\lambda)}{\partial \lambda} \right\rangle_\lambda d\lambda \quad (17)$$

In eq 17, the bracket $\langle\ \rangle_\lambda$ denotes statistical averaging over an ensemble of configurations with energies $E_i(\lambda)$. In our simulations, we used the Monte Carlo method and Metropolis sampling scheme[56,57] to model ensembles of [Mb, cyt b_5] configurations with effective energies given by eq 12**.** In this first application, the coordinates of met-Mb (lymb.pdb[28]) were fixed in the simulations, and $Fe^{3+}b_5$ (1cyo.pdb[29]) was moved as a rigid body. The coordinates of the mutants were the same as those of the native Mb, with the atomic charges of the residues adjusted to model the effect of mutations.

Because the electron transfer rate drops approximately exponentially with the distance between donor and acceptor, the effective energy computed using eq 12 is very large (positive) for most protein−protein configurations other than for the small fraction of the configurations that have the two hemes in close proximity. Thus, the MC simulation with effective energies samples a narrow region of configuration space with strong donor/acceptor electronic couplings. Because of this restricted sampling, one can use more accurate (and computationally expensive) methods to compute electronic couplings and docking interaction energies than otherwise would be accessible.

In this contribution, the linear approximation[58] is used to perform the thermodynamic integrations of eq 17. To compute the effective free energy changes associated with changes of the effective Hamiltonian from state 1 to state 2, two MC trajectories are generated, one with effective Hamiltonian 1 and the second with Hamiltonian 2. For each configuration along these two MC trajectories, the difference between effective energies 1 and 2 (determined with the corresponding Hamiltonians) are computed and averaged over the MC trajectories. In this approximation, the effective free energy difference is:

$$\Delta A^{eff}(1 \rightarrow 2) = \frac{1}{2}(\langle E^{eff}(2) - E^{eff}(1)\rangle_1 + \langle E^{eff}(2) - E^{eff}(1)\rangle_2) \quad (18)$$

Implementation of the Functional Docking Calculations. The Monte Carlo sampling with effective energies was implemented as a computational module in the HARLEM program.[59] We used the PATHWAY method[17] to compute electronic couplings in each protein configuration, with the through-space decay parameter for the interprotein coupling matrix element taken as 0.9 Å^{-1}, corresponding to $\beta = 1.8$ Å^{-1} as the decay constant for the ET rate. This value accounts for the presence of water in the space between the two proteins.[60−63] As we

(52) Zwanzig, R. W. *J. Chem. Phys.* **1954**, *22*, 1420−1426. Erratum. *J. Chem. Phys.* **1954**, *22*, 2099.
(53) Meirovitch, H. *Rev. Comput. Chem.* **1998**, *12*, 1−74.
(54) Kirkwood, J. G. *J. Chem. Phys.* **1935**, *3*, 300−313.
(55) Straatsma, T. P.; McCammon, J. A. *Annu. Rev. Phys. Chem.* **1992**, *43*, 407−435.
(56) Binder, K.; Baumgaertner, A.; Hansen, J. P.; Kalos, M. H.; Kehr, K. W.; Landau, D. P.; Levesque, D.; Mueller-Krumbhaar, H.; Rebbi, C.; Saito, Y.; Schmidt, D.; Stauffer, D.; Weis, J. J. *Top. Curr. Phys.* **1987**, *36*, 299−324.
(57) Metropolis, N.; Rosenbluth, A. W.; Rosenbluth, M. N.; Teller, A. H.; Teller, E. *J. Chem. Phys.* **1953**, *21*, 1087−1092.
(58) Sham, Y. Y.; Chu, Z. T.; Tao, H.; Warshel, A. *Proteins* **2000**, *39*, 393−407.
(59) Kurnikov, I. V. *HARLEM-Molecular Modeling Program*; http://www.kurnikov.org/harlem_main.html, 1996−2003.
(60) Jones, M. L.; Kurnikov, I. V.; Beratan, D. N. *J. Phys. Chem. A* **2002**, *106*, 2002−2006.
(61) Miller, N. E.; Wander, M. C.; Cave, R. J. *J. Phys. Chem. A* **1999**, *103*, 1084−1093.

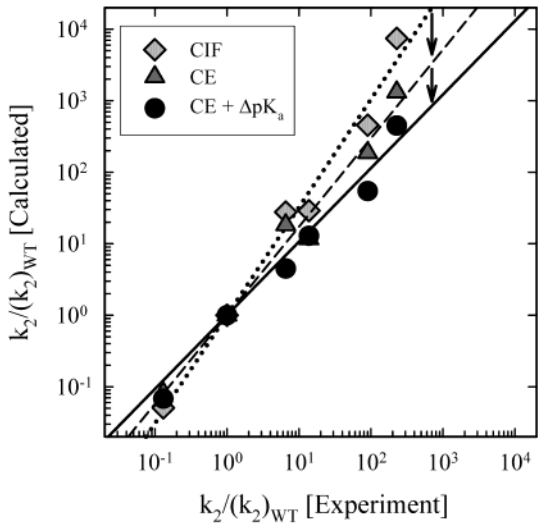

Figure 7. Experimental and theoretical rate ratios for ZnMbs (**1**−**6**) and cyt b_5. *Theoretical model*: (◇), Charges in the field; (△) continuum electrostatics; (●) continuum electrostatics with ZnMb propionate charges adjusted to give a pK_a of 6.5. *Conditions*: pH = 7.0; μ = 0.02M.

discussedabove in the Materials and Methods section, two models have been used to compute the electrostatic energies of the protein complexes: the CIF model which computes the protein−protein electrostatic interactions considering charges of one protein (cyt b_5) in the electrostatic field of the other (ZnMb) and the 3PB model in which the protein−protein electrostatic interaction energy is computed from the difference of the electrostatic energies of the protein complex and its components. The CIF model, which is also used in the conventional Brownian Dynamics simulations described earlier, allows millions of protein−protein configurations to be probed, but it does not account for desolvation energy that results from protein complex formation or for structural relaxation in the complex. The 3PB model involves Poisson−Boltzmann calculations of the electrostatic energies of the two individual proteins in water and the protein−protein "complex" (configuration) in water for each point of the MC trajectory. While this model is more accurate than the CIF model, it is more expensive. Only because of the effectiveness of the Monte Carlo/effective energy procedure is it possible to use this more expensive model in the "Functional Docking" simulations.

Functional Docking simulations of cyt b_5 and ZnMb with effective energy functions (eq 12) used MC trajectories of about 10^6 steps for the CIF model and 50,000 steps for the 3PB model. Figure S3 shows the convergence of the effective energy change averages due to mutation along the MC trajectory of each Mb (**1** → **6**) with the CIF electrostatic model. The results show that 50,000 step trajectories are sufficient for convergence of the effective energy changes, within 5−10%. More sophisticated methods to generate MC trajectories (such as the replica exchange method)[64] may allow a further decrease in the number of MC steps needed to achieve convergence.

Monte Carlo Docking Simulations. Results. Changes in the bimolecular ET rate constant, k_2, computed with eq 14 for the suite of ZnMbs (**1** → **6**) are shown in Figure 7. Calculations with the CIF model and protonation states derived from experimental pK_a values show a reasonable agreement with experiment. They yield an exponential dependence of the bimolecular, ^{3}ZnMb → cyt b_5 ET rates on the nominal charge of the myoglobin, and the computed changes of the logarithms of the ET rate constants are overestimated by 50−80%. Given the crude method for calculating binding energies, this modest overestimate is inevitable: the computations do not incorporate relaxation and desolvation effects which must moderate the real changes. As anticipated, calculations with the more accurate "3PB" interaction model show an improved agreement between the theoretical and experiment results; now the theoretically predicted logarithms of the relative bimolecular ET rate constant changes are overestimated by 20−40%. Clearly, such agreement with relatively low-level binding-energy calculations both support the model and point the way to improvements that are only feasible because of the computational efficiency of the algorithm.

Figure 8 shows the protein configurations sampled in the FD runs for Mb (**2**). The "dots", which represent the positions of the Fe atoms of cyt b_5 in complexes that contribute to k_2 (right), all belong to a relatively small region of configuration space and propionates of the two partner proteins are in close spatial proximity in which the Mb surface has high reactivity, as shown by their overlap with the reactive area of the PATHWAYS ET coupling map. The compactness of the distribution of cyt b_5 configurations in this "ET biased" FD trajectory reflects the narrowness of the strongly ET coupled region of the surface of ZnMb. Even so, no single protein configuration dominates electron transfer—many configurations that differ substantially in the relative orientation of the two proteins have similar values of the effective energy, and contribute comparably. On the top left is an alternate computation designed to examine binding, *not* reaction. It presents a FD run in which the effective energies were set to depend *not* on the coupling, but to increase linearly with the *minimal* atom−atom distance between two proteins for *all* bound configurations, independent of the coupling (the apparent k_{et}^i decrease exponentially with protein−protein distance), and thus the k_{et}^i are similar for all bound configurations; positions of the Fe atoms of cyt b_5 from configurations of these "ET-non biased" FD trajectories are overlaid with the isopotential electrostatic potential surface of Mb (**2**).

The plot shows that the reactive conformations indeed represent only a small fraction of the configurations that contribute to binding. One can see that the lack of specificity in the interaction of cyt b_5 with Mb (**2**) is due to intermittent regions of positive and negative potential around Mb, in sharp contrast with the compactness of the distribution of the cyt b_5 configurations in the "ET-biased" MC trajectory. These results are in qualitative agreement with the BD computations.

The analogous computations for Mb(S92D) (**1**), shown in Figure 8 upper, are quite similar to those of Mb (**2**) in representing Dynamic Docking, showing an even broader distribution of bound configurations, while again showing a cluster of reactive configurations near the Mb heme edge. The comparable pair of computations for the charge-neutralized mutant, [V67R]Mb(dme) (**6**), with $\Delta q_{nom} = +3$ show that here too the *reactive* region of configuration space is minimally changed. However, the "ET-nonbiased" profile which emphasizes binding has shifted such that the docked configurations

(62) Ponce, A.; Gray, H. B.; Winkler, J. R. *J. Am. Chem. Soc.* **2000**, *122*, 8187−8191.
(63) Page, C. C.; Moser, C. C.; Chen, X.; Dutton, P. L. *Nature (London)* **1999**, *402*, 47−52.
(64) Sugita, Y.; Kitao, A.; Okamoto, Y. *J. Chem. Phys.* **2000**, *113*, 6042−6051.

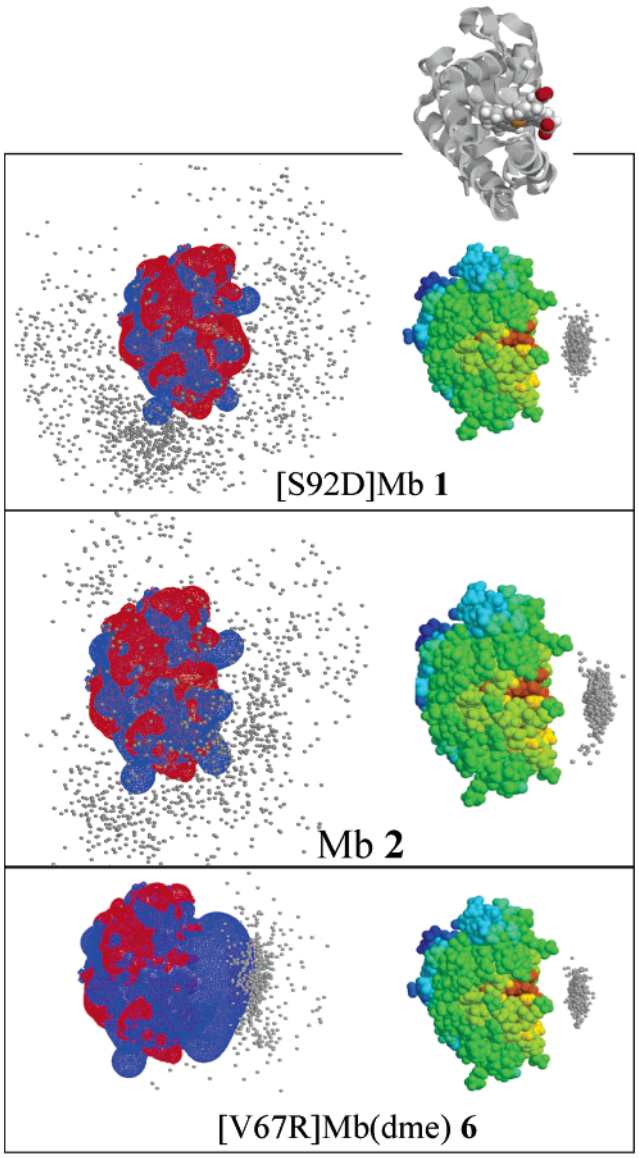

Figure 8. Monte Carlo simulations for (**1**), (**2**), and (**6**). Points represent the position of the Fe atom of cyt b_5 in ~500 configurations taken from a long (>10^6 steps) MC trajectory. (Left**)** Overlay of electrostatic isopotential surfaces (+1 kT and −1 kT) and the trajectory *without* ET bias; effective energy depends linearly upon the minimal distance between atoms of the two proteins for each protein−protein configuration (see text). **(**Right**)** Functional Docking computation with effective energy given by eq 12; overlay of ET coupling surface map and the Functional Docking trajectory.

now cluster near the heme face, where the [V67R]Mb(dme) (**6**) electrostatic field shows a strongly attractive positive potential. Again, similar *qualitative* docking profiles were obtained in the BD calculations, Figures 5 and S2.

These calculations for the [S92D]Mb (**1**) and [V67R]Mb-(dme) (**6**) mutants, which represent the extremes of the charge-varying suite of six Mbs, thus show that effective-energy MC computations inherently exhibit the fundamental features of the DD landscape, a decoupling of binding and reactivity, without ad hoc assumptions.

Because ET between ZnMb and cyt b_5 is so strongly influenced by the charges of the heme propionates and the surface residues at the protein−protein interface in the ET active configurations, it is important to consider carefully how the protonation equilibrium of the titratable residues might affect

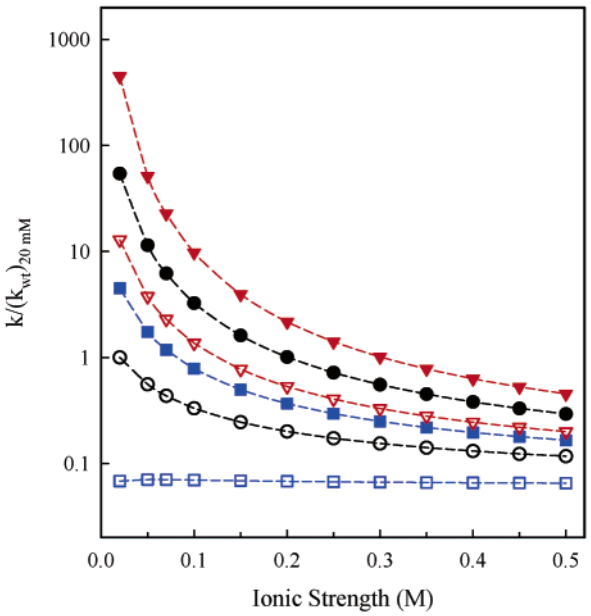

Figure 9. Ionic strength dependence of the bimolecular rate constants for the ET reaction between ZnMb and cyt b_5 computed with the Functional Docking algorithm (relative to WT ZnMb at 0.02 M ionic strength). *Derivatives*: (○) native ZnMb (**2**); (□) [S92D]Mb (**1**); (▽) [V67R]Mb (**3**); (■) [S92D]Mb(dme) (**4**); (●) Mb(dme) (**5**); (▼) [V67R]Mb(dme) (**6**).

the computed ET rate constant changes. We computed changes in the pK_a values of the histidine residues and heme propionates for 100 points randomly chosen on the MC trajectory (with WT myoglobin) and compared them with the pK_a values computed for the isolated proteins in water (Figure S4). The calculations predict that the pK_a of the ZnMb and cyt b_5 heme propionates are substantially raised (shifted toward the neutral state) in the ET-active configurations as compared to the isolated proteins. Significant pK_a shifts are also obtained for the heme ligand (His 93), the distal His (His 64), and for His 97 which is involved in a H-bond link to the propionate of the Mb heme. A rigorous treatment of the pK_a changes in MC calculations would require recomputation of pK_a values at each point in the MC trajectories and proper calculations of free energy terms associated with changes of charge distribution associated with pK_a changes. At present, this kind of calculation remains beyond our abilities. Therefore, to evaluate the effect of dynamical pK_a changes on computed ET rate changes, we shifted the propionate pK_a values of ZnMb and cyt b_5 from 4.5 to 6.5 and repeated the MC computations of the bimolecular ET rate changes for each of the six mutants. The results of these calculations (Figure 7) agree well with experiment. The faster ET rates for [V67R]Mb (**3**) compared to [S92D]Mb(dme) (**4**) (which has the same (+1e) nominal change of charge relative to Mb (**2**)) is well described. The bimolecular ET rates for the [V67R]Mb(dme) derivative (**6**) are still somewhat overestimated in these calculations.

The computed ionic-strength dependences for the bimolecular ET rate between ^{3}ZnMb and cyt b_5 (3PB electrostatic model with shifted pK_a values for the heme propionates) are shown in Figure 9 for each of the six Mbs (**1** → **6**). In agreement with experiment, the calculations predict a strong decrease in the relative k_2 values with increasing salt concentration as the formal charge on Mb becomes increasingly positive. The bimolecular ET rate of the [S92D]Mb derivative (**1**) shows a weak dependence on ionic strength, even though the formal charge

of the [S92D]Mb derivative is negative at pH 7.0 (even with the pK_a of the propionates shifted to 6.5), and it may be expected that the bimolecular ET rates for the [S92D]Mb derivative would increase with increasing ionic strength. As suggested above, the nonuniformity of the atomic charge distribution must clearly be taken into account to describe the ionic-strength dependence of protein−protein interactions.

The magnitudes of the predicted decreases in ET rates with ionic strength for the Mb derivatives with the large nominal positive charge are somewhat overestimated compared to experiment, probably reflecting the deficiency of the rigid protein model used in the current simulations. In the experiment, charged surface groups (including heme propionates) have substantial freedom to move and will respond to changes in electrostatic conditions (analogously with ions in solution). Thus, the flexibility of charged protein groups should reduce the ionic-strength dependence of protein−protein interactions and ionic-strength dependence of bimolecular ET rates. Another effect that diminishes the dependence of bimolecular ET rates on the ionic strength is the change of pK_a values of titratable groups. Recent NMR studies[65] have demonstrated that the pK_a values of the surface histidines for Mb (**2**) increase by 0.16 to 0.64 units as the ionic strength increases from 0.02 to 1.0 M. One sees from results presented in Figure 9 that "Functional Docking" calculations qualitatively reproduce the approximate differences in the saturation levels of the ET rates at high [NaCl]. The favorable agreement between the theoretical and experimental rate ratios supports the underlying assumptions of the DD description of ^{3}ZnMb → $Fe^{3+}b_5$ ET.

Discussion

We have used myoglobin (Mb) as a convenient "workbench" to probe the effects of electrostatics on binding and reactivity in the dynamic [Mb, cyt b_5] complex. Through combination of mutagenesis and heme neutralization we have produced a suite of six Mb surface-charge variants whose nominal charge ranges from −1 to +3 units relative to that for native Mb (Table 1). The replacement of S92 in Mb with a negative aspartate, or the replacement of V67 with a positive arginine are known to have a negligible effect on the structure and electrochemical properties of Mb.[24,25] Likewise, NMR and kinetic studies show that methylation of the heme propionates has a minimal effect on the structure.[66,67] Our NMR studies [16] further indicate that zinc-deuteroporphyrin IX, with its propionates neutralized, is locked in the heme pocket, as is the heme of native Mb (with one propionate hydrogen-bonded to Ser92 and shielded from the solvent, while the other protrudes into the solvent and remains flexible).

For each member of the suite, we have measured the bimolecular quenching rate constant (k_2) for the photoinitiated, ^{3}ZnDMb → $Fe^{3+}b_5$ ET reaction as a function of ionic strength. The ET rate constant responds dramatically to variations in the Mb surface charge. As we reported previously,[14] neutralization of the heme propionates, giving $\Delta q_{nom} = +2$, enhances k_2 by ∼60-fold. We see analogous behavior when we use site directed mutagenesis to vary the nominal charge from −1 to +1, with introduction of negative charge(s) to the Mb surface decreasing k_2, while positive charge(s) increase k_2. Combining these two approaches to give $\Delta q_{nom} = +4$ gives an even more remarkable increase in k_2 by a factor of ca. 2×10^3, from [S92D]ZnMb (**1**) with $q_{nom} = -1$ to [V67R]ZnMb(dme) (**6**) with $q_{nom} = +3$. For comparison, a double-charge mutation in cyt *c* produced only a ∼5-fold change in k_2 for the reaction with cyt b_5.[3]

Previously,[14] we showed that neutralization of the Mb heme propionates does not significantly enhance Mb's binding affinity for cyt b_5: for the neutral ZnMb(dme) (**5**) and ZnMb-(diamide), K_a (ITC) = 540 ± 80 M^{-1} and K_a (NMR) ∼ 500−1000 M^{-1}, respectively; for the native ZnMb (**2**), K_a (ITC) = 350 ± 70 M^{-1}. We now find this effective decoupling throughout the Mb suite. The titration curves of the new members of the Mb suite remain linear (Figure 3), and simulations show that this requires that for these, too, $K_a \lesssim 500-1000$ M^{-1}. Thus K_a varies by less than 2−3-fold while k_2 varies by *3 orders of magnitude*. Previous paradigms for protein−protein ET cannot accommodate such findings. Instead these results show that the [ZnMb, $Fe^{3+}b_5$] complex is described by the DD landscape (Figure 1), and the ET process by the resulting kinetic equations: eqs 2a, 2b, and 3c.

Equations 2a, 2b, and 3c are obtained in the "reaction" (rapid-exchange) limit, but the second-order kinetics implied by the linear titration curves are compatible either with rapid-exchange by a weakly bound complex at low concentration *or* with the opposite limit of a diffusion-controlled ("collisional") reaction. We argued that the former limit does apply, and the availability of a sufficiently large suite of charge variants supports those arguments. In the diffusion limit, the low ionic strength value for k_2 should vary linearly with Mb charge,[46] contrary to experiment (Figure 6). In contrast, DD kinetic equations in the rapid-exchange limit predict that ln k_2 is proportional to Mb charge, in full agreement with experiment (Figure 6). The prediction arises as follows. In the DD model, k_2 is dominated by the minority reactive configurations, $k_2 \approx k_2^R$, which is proportional to the binding constant for the reactive configurations, eq 3c. As a result, in this limit, ln $k_2^R \propto$ ln $K_a^R \propto -\Delta G_b^R/kT$, where ΔG_b^R is the binding free energy for the reactive configurations.

When the binding free energy is dominated by electrostatic interactions, as had long been recognized for this complex, $\Delta G_b^R \propto Z_{Mb}$ (the Mb charge); this is explicitly seen in the Debye−Hückel treatment, where ln $k_{20} \propto V(Z_{Mb}), \propto Z_{Mb}$, eq 7. The calculated net charge on the Mbs varies in proportion to Δq_{nom}, with a slope of nearly unity. The linear variation of log k_{20} (or equivalently, log k_2 at 18 mM ionic strength) with Δq_{nom} **(**Figure 6**)** completes the demonstration that the [Mb, $Fe^{3+}b_5$] complex exemplifies the DD paradigm. Deviations from unit slope are largely attributable to changes in residues pK_a values computed using the Tanford−Kirkwood algorithm. However, we cannot rule out a small contribution from gating[12] *within* the minority reactive configurations.[68,69]

The BD simulations and PATHWAY calculations illuminate as well as support the DD picture in which "charge neutralization" enhances reactivity by increasing the probability of binding

(65) Kao, Y. H.; Fitch, C. A.; Bhattacharya, S.; Sarkisian, C. J.; Lecomte, J. T. J.; Garcia-Moreno, B. *Biophys. J.* **2000**, *79*, 1637−1654.
(66) La Mar, G. N.; Emerson, S. D.; Lecomte, J. T. J.; Pande, U.; Smith, K. M.; Craig, G. W.; Kehres, L. A. *J. Am. Chem. Soc.* **1986**, *108*, 5568−5573.
(67) Hunter, C. L.; Lloyd, E.; Eltis, L., D.; Rafferty, S. P.; Lee, H.; Smith, M.; Mauk, A. G. *Biochemistry* **1997**, *36*, 1010−1017.
(68) Zhou, H.-X.; Wong, K.-Y.; Vijayakumar, M. *Proc. Natl. Acad. Sci. U.S.A.* **1997**, *94*, 12372−12377.
(69) Zhou, H.-X. *Biopolymers* **2001**, *59*, 427−433.

in a reactive configuration. The BD simulations show that the total number of hits increases minimally as the charge on Mb increases from [S92D]ZnMb (**1**) to [V67R]ZnMb(dme) (**6**), whereas the number of hits with high ET reactivity, those with cyt b_5 docked to the Mb surface near the heme edge, dramatically increases in parallel with Δq_{nom} (Figures 5 and S2). Consequently, the reactive surface of Mb determined from PATHWAY coupling calculations is sharply restricted to the vicinity of the heme edge for all six variants, indicating that the ET reactivity of the Mb surface is not significantly altered by changes in the surface charge.

Monte Carlo Functional Docking (FD) Calculations. The correlation of the experimental rate constants with Brownian Dynamics and ET PATHWAY analysis illuminates and provides qualitative support for the DD model for ET between Mb and cyt b_5. The new "Functional Docking" algorithm gives a novel, quantitative, predictive method for calculating ET rate constants, and the success of these computations further confirms the applicability of the DD model to the [Mb, $Fe^{3+}b_5$] complex. The FD method mathematically links binding and ET *during* computations, not after, through the definition of the effective energy, E_{eff} (eq 12). Monte Carlo FD simulations with effective energies have a clear advantage in exploring bimolecular ET reactions controlled by a small sub-population of conformers in rapid-exchange as compared to Brownian Dynamics and standard Monte Carlo docking procedures that use "normal" interaction energies. In a FD computation, only a relatively small number of protein−protein configurations (those with strong donor−acceptor couplings) need to be analyzed to compute the relative rate constants. Because of the restricted sampling, more realistic and computationally demanding coupling and docking energy analysis can be employed. The FD simulations provide a quantitative tool to analyze factors that control the bimolecular ET reaction rate. Even in this first application, with relatively crude methods of evaluating binding energy and donor/acceptor couplings, the method reproduces the observed dependence of the bimolecular ET rates on Mb surface charge and ionic strength. We plan to use this approach to explore how intermolecular ET is influenced by surface group mobilities, hydrophobic interactions, and bridging water.

The computations reported here are limited to bimolecular ET reactions in the "rapid-exchange" regime, appropriate when interacting molecules have small binding energies or small ET rates. If the binding energies of configurations with strong ET couplings are increased by changes in solution conditions or chemical modifications, or if the ET rates are large, the "rapid-exchange" regime becomes invalid and explicit consideration of protein diffusion is essential (e.g., refs 68 and 69). It is expected, for example, that further increases of the positive Mb surface charge will result in a smaller relative increase in the ET rate constant because the reaction will become rate limited by protein diffusion. A combination of Monte Carlo and Brownian Dynamics simulations will be useful to investigate bimolecular ET reactions in the regime intermediate between activation and diffusion control.

Why does the [Mb, cyt b_5] complex exhibit a DD landscape? Electrostatic interactions between Mb and cyt b_5 play a more important role in directing "productive" protein docking than in contributing to the overall binding free energy of the complex. Indeed, studies of a wide variety of protein−protein interactions indicate that large binding affinity and/or kinetic barriers for binding/unbinding are usually associated with hydrophobic interactions and with specific interactions such as hydrogen bonds and salt bridges.[70−73] Two protein partners probably need to have considerable shape complementarity to have a large number of strong and specific binding interactions. However, cyt b_5 is "football-shaped", with one of the heme propionates at the "tip", and it is clear that cyt b_5 and Mb do not have optimal shape-complementary binding interface. Therefore, even when electrostatic interactions favor binding between Mb and cyt b_5, as evidenced by the ionic strength dependence of k_2, (Figure 4), a poor shape complementarity probably acts to limit the formation of the hydrogen bonds, salt bridges, and hydrophobic interactions between Mb and cyt b_5 that would most effectively stabilize a complex.

Protein−protein interactions are of fundamental importance not only to electron transfer[5,74−76] but also to many other cellular processes,[50] including signal transduction[77,78] and metal-ion trafficking,[79,80] and it seems likely to us that the DD paradigm will apply to many other complexes. Indeed, some of the protein−protein interactions involved in these other processes seem to have high specificity but modest binding affinity, which is prerequisite for fast signal or substrate transfer.[36,77,81] Unlike tightly bound protein−protein complexes where hydrophobic contacts dominate, the interactions between the protein partners in weakly bound complexes tend to be dominated by long-range electrostatic interactions. This is perhaps because electrostatic interactions play a more important role in guiding the formation of a "productive complex" than in contributing to the overall binding energy, as our results have indicated. On the basis of this framework for understanding docking interactions, it is plausible to suggest that, in order for protein partners to achieve high specificity and low binding affinity, they need to have optimized electrostatic complementarity with poor shape complementarity (to avoid hydrophobic packing, formation of hydrogen bonds, and salt bridges).

Summary

We have reported studies of photoexcited ET from ZnMb to $Fe^{3+}b_5$, within the suite of Mb charge variants. We find: (i) a dramatic decoupling of binding and reactivity, in which k_2 varies $\sim 10^3$-fold within the suite of Mbs without a significant change in binding affinity; (ii) the ET reaction occurs within the "thermodynamic" or "rapid exchange" limit of the dynamic-docking model, as shown by the fact that the zero-ionic-strength bimolecular rate constant varies exponentially with the net charge on Mb; (iii) Brownian Dynamics docking profiles and PATHWAYS calculations support this analysis and allow us to visualize the microscopic basis of Dynamic Docking.

(70) Jones, S.; Thornton, J. M. *Proc. Natl. Acad. Sci. U.S.A.* **1996**, *93*, 13−20.
(71) Stites, W. E. *Chem. Rev.* **1997**, *97*, 1233−1250.
(72) Norel, R.; Petrey, D.; Wolfson, H. J.; Nussinov, R. *Proteins: Struct., Funct., Genet.* **1999**, *36*, 307−317.
(73) Conte, L. L.; Chothia, C.; Janin, J. *J. Mol. Biol.* **1999**, *285*, 2177−2198.
(74) Mauk, A. G. *Essays Biochem.* **1995**, *34*, 101−124.
(75) Kostic, N. M. *Metal Ions Biol. Syst.* **1991**, *27*, 129−182.
(76) Nocek, J. M.; Zhou, J. S.; Hoffman, B. M. *J. Electroanal. Chem.* **1997**, *438*, 55−60.
(77) Pawson, T.; Scott, J. D. *Science* **1997**, *278*, 2075−2080.
(78) Downward, J. *Nature (London)* **2001**, *411*, 759−762.
(79) Rosenzweig, A. C. *Acc. Chem. Res.* **2001**, *34*, 119−128.
(80) Lamb, A. L.; Torres, A. S.; O'Halloran, T. V.; Rosenzweig, A. C. *Nat. Struct. Biol.* **2001**, *8*, 751−755.
(81) Pelletier, H.; Kraut, J. *Science* **1992**, *258*, 1748−1755.

Our results thus confirm that the "Dynamic Docking" paradigm describes the [Mb, cyt b_5] ET reaction: *Multiple weakly bound conformations of the docked complex contribute to the binding of cyt b_5 to Mb, but only a limited subset of these conformations are ET active*. This paradigm differs from the more familiar picture where binding strength and ET reactivity increase in parallel. Rather, the Dynamic Docking mechanism obviates the need for tight binding to achieve efficient ET reactivity, in effect decoupling binding from reactivity. Such decoupling clearly is of physiological relevance for the reduction of met-Hb in red blood cells, where tight binding of cyt b_5 to the large population of ferrous-Hb would prevent the cytochrome from finding and reducing additional metHb.

To describe this situation we have developed a new, computationally efficient, Monte Carlo docking procedure with an effective energy function that mathematically links the intermolecular interaction energies and electron transfer rates. This Functional Docking algorithm provides an effective computational tool to study bimolecular ET reactions. This new approach successfully describes the effects of mutations in varying the second-order ET rate constant and ionic strength profiles.

Acknowledgment. The work is supported by the National Institutes of Health (HL62303 [B.M.H.]) and GM48043[DB]) and by the Protein Engineering Network of Centres of Excellence (A.G.M.). We thank Mr. Steven Lowe for his help with the Brownian Dynamics simulations.

Supporting Information Available: Additional figures (PDF). This material is available free of charge via the Internet at http://pubs.acs.org.

JA038163L